ELSEVIER

Journal of Wind Engineering
and Industrial Aerodynamics 67&68 (1997) 65–78

JOURNAL OF wind engineering AND industrial aerodynamics

Calculation of the flow past a surface-mounted cube with two-layer turbulence models

D. Lakehal, W. Rodi*

Institute for Hydromechanics, University of Karlsruhe, Kaiserstrasse 12, D-76128 Karlsruhe, Germany

Abstract

In 3-D steady calculations of the flow around a cube placed in developed-channel flow, various versions of the k–ε model were tested. For the near-wall treatment, standard wall functions were employed, as well as the two-layer approach in which the viscous sublayer is resolved with a one-equation model. Two versions of the one-equation model were tested. In addition, calculations were carried out with the Kato–Launder (1993) modification of the k–ε model which eliminates excessive turbulence production in stagnation regions. The various predictions are compared with the measurements of Martinuzzi and Tropea (1993).

Keywords: Cube; Three-dimensional; Channel-flow; Turbulent; Two-layer model

1. Introduction

The standard k–ε two-equation model using wall functions to bridge the viscous sublayer is the most commonly used turbulence model in practice and has been found to work well in many simpler flow situations, mainly of the shear-layer type. However, in more complex situations involving impingement and separation regions which are always present in the flow around buildings, the use of the isotropic eddy-viscosity concept and of wall functions has revealed deficiencies. Isotropic eddy-viscosity models produce excessive turbulent kinetic energy in impingement regions due to an unrealistic simulation of the normal turbulent stresses which contribute most to the turbulence production in such regions. An ad hoc modification of the k–ε model proposed by Kato and Launder [1] which eliminates the excessive production is tested in this paper. Wall functions are based on the assumption of a logarithmic velocity distribution and of local equilibrium of turbulence at the first grid point placed outside the viscous sublayer. These assumptions are clearly not valid in

* Corresponding author. E-mail: Rodi@ifh.bau-verm.uni-karlsruhe.de.

PII S0167-6105(97)00063-9

separation regions. Therefore, considerable effort has been devoted in the last 10 years to the development and testing of low-Reynolds-number versions of the k–ε model with which the viscous sublayer can be resolved, and many different variants have been proposed [3]. Extensive testing has shown (see, e.g., Ref. [4]) that these models clearly improve the calculations of 2-D separated flows over the use of wall functions, but they have the disadvantage of requiring a high grid resolution in the viscous sublayer (25 to 30 grid points) because of the steep gradients of ε very near the wall. This leads to resolution problems in geometrically complex situations involving a number of walls. Also, basically all variants overpredict turbulence and, consequently, the friction coefficient in adverse pressure gradient boundary layers.

As an alternative, the two-layer approach has recently become popular, in which only the core flow outside the viscosity-affected near-wall region is simulated by the k–ε model. The viscous sublayer is resolved by a simpler model, notably a one-equation model in which the length-scale distribution is prescribed and an ε-equation is not solved. Such models therefore require considerably fewer grid points in the viscous sublayer, of the order of 10–15, and are therefore more suitable for complex situations involving more than one wall for which the near-wall regions have to be resolved. Also, because of the fixed length-scale distribution near the wall, these models have been found to give better predictions for adverse pressure gradient boundary layers than pure k–ε models. A review on the work up to 1990 in this area can be found in Ref. [5].

The objective of this paper is to test various two-layer models, which differ in the near-wall one-equation model used, and also the Kato–Launder modification vis-à-vis the standard k–ε model using wall functions for the flow around a simple building. The flow around a surface-mounted cube placed in a developed channel flow was chosen because (i) it has a simple geometry but has all the important complex features of real building flows as described briefly in Section 2 below, (ii) it was studied experimentally in detail by Martinuzzi and Tropea [2] and (iii) the boundary and inflow conditions are well defined. A further advantage is that LES results are available for comparison [6].

2. Flow around a surface-mounted cube: the experimental study [2]

The geometry of the test case is sketched in Fig. 1. The height of the cube is half of that of the channel. For $\mathrm{Re} = U_B H/\nu = 40\,000$ (U_B is the bulk velocity, H is the cube height) Martinuzzi and Tropea [2] carried out flow visualization studies and detailed LDA measurements from which the mean velocity components and the various Reynolds stresses are available. The entry section of the channel was long enough to have developed channel flow. The on-coming turbulence intensity at roof height is relatively low ($T_u = \sqrt{u'^2}/U_B \approx 0.03$). From their flow visualization studies and the detailed measurements, Martinuzzi and Tropea devised the flow picture given in Fig. 2 which clearly shows the very complex nature of the flow in spite of the simple geometry. The flow separates in front of the cube; on average there is a primary separation vortex but also a secondary one, while instantaneously up to four

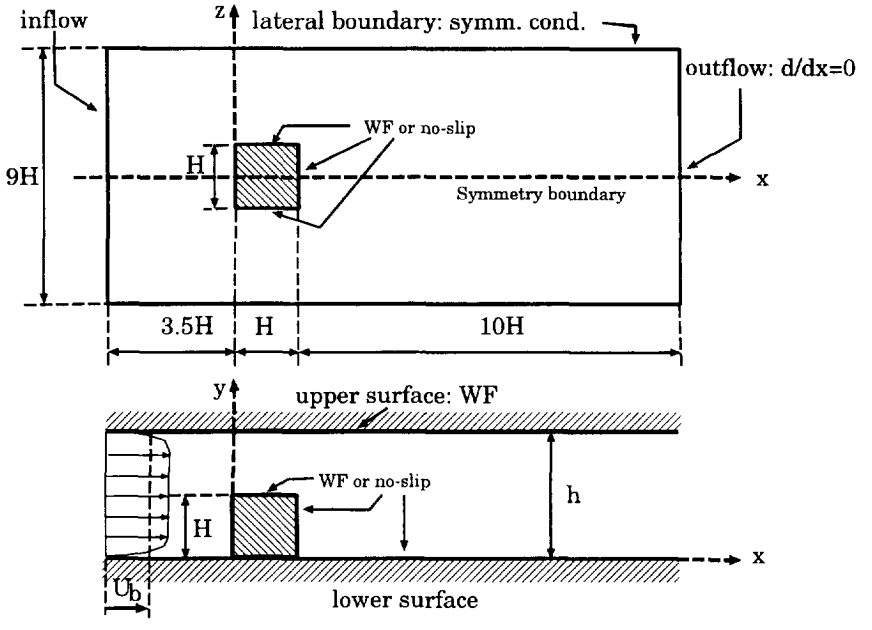

Fig. 1. Geometry of the test case and boundary conditions.

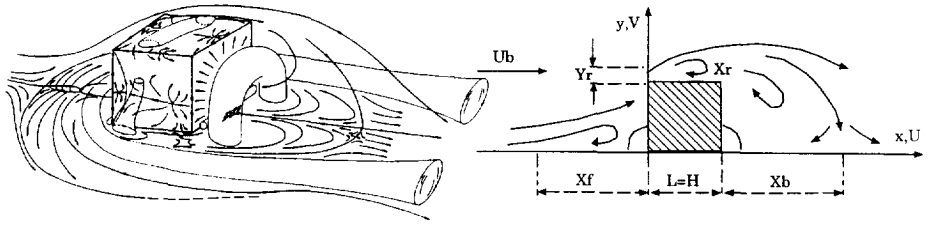

Fig. 2. Schematic representation of the flow around a cube from Ref. [2].

separation vortices were detected. The main vortex wraps as a horse-shoe vortex around the cube into the wake and has a typical converging-diverging behaviour. The flow separates at the front corners of the cube on the roof and the side walls; on average it does not reattach on the roof but there appears to be reattachment on the side walls. A large separation region develops behind the cube which interacts with the horse-shoe vortex. Originating from the ground plate, an arch vortex develops behind the cube. Predominant fluctuation frequencies were detected sideways behind the cube, which were traced to vortex shedding of the flow past the side walls. The Strouhal number was found to be $St = f/HU_B = 0.15$. Further, bimodal behaviour of the flow separation, and, in particular, of the vortices in front and on the roof was

observed. Of course, such unsteady phenomena cannot be accounted for in the steady-calculation procedure used in the present study, which may be responsible for some of the discrepancies to be discussed below.

3. Standard k–ε model and Kato–Launder modification

The standard k–ε model [7] employs the Boussinesq eddy-viscosity concept and determines the isotropic eddy viscosity ν_t from

$$\nu_t = C_\mu k^2/\varepsilon. \tag{1}$$

The distributions of k (turbulent kinetic energy) and ε (dissipation rate) appearing in this relation are determined from the following model transport equations:

$$(U_i k)_{,i} = \left[\left(\nu + \frac{\nu_t}{\sigma_k}\right)k_{,i}\right]_{,i} + P_k - \varepsilon;$$

$$(U_i \varepsilon)_{,i} = \left[\left(\nu + \frac{\nu_t}{\sigma_\varepsilon}\right)\varepsilon_{,i}\right]_{,i} + C_1 P_k \varepsilon/k - C_2 \varepsilon^2/k, \tag{2}$$

$P_k = \overline{u_i u_j} U_{i,j}$ represents the rate of production of turbulent kinetic energy resulting from the interaction of turbulent stresses and mean velocity gradients. The model employs the following standard values of the empirical constants: $C_\mu = 0.09$; $C_1 = 1.44$; $C_2 = 1.92$; $\sigma_k = 1.0$ and $\sigma_\varepsilon = 1.3$. In the standard version of the model, wall functions are used which relate the velocity parallel to the wall, as well as k and ε at the first grid point to the friction velocity [7].

The isotropic eddy-viscosity concept used in the k–ε model leads to an unrealistically high production of k in the stagnation regions occurring in impinging flows. This is a consequence of the inability of these models to simulate correctly the difference between normal stresses governing the production P_k in such regions. Kato and Launder [1] suggested as an ad hoc measure to replace the original production term $P_k = C_\mu \varepsilon S^2$ by $P_k = C_\mu \varepsilon S\Omega$, where $S = k/\varepsilon\sqrt{1/2(U_{i,j} + U_{j,i})}$ and $\Omega = k/\varepsilon\sqrt{1/2(U_{i,j} - U_{j,i})}$ denote, respectively, the strain and vorticity invariants. In simple shear flows the behaviour remains unchanged as $\Omega \approx S$ while in stagnation regions $\Omega \approx 0$ so that the spurious turbulence production is eliminated.

4. Two-layer turbulence models

4.1. Basic concept

The two-layer approach adopted here consists of resolving the viscosity-affected regions close to walls with a one-equation model, while the outer core flow is resolved with the standard k–ε model described above. In the one-equation model, the eddy viscosity is made proportional to a velocity scale and a length scale l_μ. The

distribution of l_μ is prescribed algebraically while the velocity scale is determined by solving the k-equation (as in Eq. (2)). The dissipation rate ε appearing as a sink term in the k-equation is related to k and a dissipation length scale l_ε which is also prescribed algebraically. The different two-layer versions available in the literature differ in the use of the velocity scale and the way l_μ and l_ε are prescribed. It should be mentioned that in the fully turbulent region the length scales l_μ and l_ε vary linearly with distance from the wall. However, in the viscous sublayer, l_μ and l_ε deviate from the linear distribution in order to account for the damping of the eddy viscosity and the limiting behaviour of ε at the wall.

4.2. $k^{1/2}$ *velocity-scale-based model* [5]: *TLK*

The approach combines the standard k–ε model in the outer region with a one-equation model due to Norris and Reynolds [8] in the viscous-sublayer employing

$$\nu_t = C_\mu k^{1/2} l_\mu; \quad \varepsilon = k^{3/2}/l_\varepsilon. \tag{3}$$

In this model, the length scale l_μ is damped in a similar way as the Prandtl mixing length by the Van Driest function, so that it involves an exponential reduction governed by the near-wall Reynolds number $R_y = \tilde{U} y_n/\nu$. However, in contrast to the original Van Driest function, R_y uses $k^{1/2}$ as a velocity scale $\tilde{U}$ instead of U_τ which can go to zero for separated flows.

$$l_\mu = C_l y_n f_\mu \quad \text{with} \quad f_\mu = 1 - \exp\left(-\frac{R_y 25}{A_\mu A^+}\right). \tag{4}$$

The constant C_l is set equal to $\kappa C_\mu^{-3/4}$ to conform with the logarithmic law of the wall. The empirical constants appearing in the f_μ-function are assigned the values $A_\mu = 50.5$ and $A^+ = 25$. The reader is referred to Ref. [5] for a review and further details on the choice of the constants. For the dissipation scale the following distribution is used near the wall:

$$l_\varepsilon = \frac{C_l y_n}{1 + C_\varepsilon/(R_y C_l)}, \quad C_\varepsilon = 13.2. \tag{5}$$

The outer (k–ε) and the near-wall model are matched at a location where the damping function f_μ reaches the value 0.95, i.e., where viscous effects become negligible.

The combination of the Kato–Launder correction with the TLK model is hereafter labeled TLKK.

4.3. $(v'^2)^{1/2}$ *velocity-scale-based model* [9]: *TLV*

The development of this model was motivated by the fact that the length scale functions as proposed in Ref. [8], particularly the l_ε-function, are not in agreement with direct numerical simulation (DNS) data, and that the normal fluctuations $(v'^2)^{1/2}$ are a more relevant velocity scale for the turbulent momentum transfer near the wall

than $k^{1/2}$. Therefore, the following model using $(v'^2)^{1/2}$ as a velocity scale was proposed in Ref. [9]:

$$\nu_t = \sqrt{\overline{v'^2}}\, l_{\mu,v}, \quad \varepsilon = \sqrt{\overline{v'^2}}\, k/l_{\varepsilon,v}, \tag{6}$$

with

$$l_{v,\mu} = 0.33 y_n, \quad \text{and} \quad l_{\varepsilon,v} = 1.3 y_n \Big/ \left[1.0 + 2.12\, v \Big/ \sqrt{\overline{v'^2}}\, y_n \right], \tag{7}$$

which is based on DNS data for fully developed-channel flow. As an equation for k is solved, $\overline{v'^2}$ needs to be related to k, which is done through the following DNS-based empirical relation:

$$\overline{v'^2}/k = 4.65 \times 10^{-5} (R_y)^2 + 4.00 \times 10^{-4} R_y, \quad R_y = k^{1/2} y_n / v, \tag{8}$$

valid only very near the wall. The matching between the outer and near-wall model is performed at a location where $R_y = 80$.

5. Outline of the computational method

The computer code FAST–3D [10] used for the flow calculations is based on a finite-volume approach for solving the incompressible Navier–Stokes equations. Flows around complex geometries can also be treated since the code is written for curvilinear body-fitted coordinates using Cartesian velocity components. A non-staggered, cell-centred grid arrangement is used. Pressure field oscillations are avoided by means of the momentum interpolation technique due to Rhie and Chow [11]. The pressure–velocity coupling is achieved using the SIMPLE algorithm. The diffusion fluxes are approximated by central differences, while the hybrid linear-parabolic approximation, a second-order low-diffusive and oscillation-free scheme of Zhu [12], is applied for the convection fluxes. The resulting system of difference equations is solved using the strongly implicit solution procedure of Stone [13].

6. Grids and boundary conditions

The computational domain with the various boundaries is shown in Fig. 1. The effect of the location of the inflow and outflow boundaries and of the lateral boundaries was studied and the boundaries were placed at the locations given in Fig. 2 to avoid any influence on the calculations. Because of symmetry conditions, only half of the width of the flow needed to be calculated. Calculations using various grids indicated that with the standard k–ε model using wall functions, grid-independent results could be obtained with $110 \times 32 \times 32$ grid points in the x-, y- and z-directions. A finer mesh consisting of $142 \times 84 \times 64$ grid points was applied in all two-layer computations. The grids were non-uniform, being considerably finer in the near-wall regions. The first cells adjacent to the walls were set with respect to the criteria

required for the individual near-wall treatment. Hence, using wall functions the width of the near-wall cell was $0.01H$ and using the two-layer approach $0.001H$, which corresponds to $10 < y^+ < 25$ and $1 < y^+ < 5$, respectively. In the two-layer case, the number of grid points placed in the viscous sublayer was in most regions typically 15–20. The boundary conditions employed are also indicated in Fig. 1: On the ground plate and the cube walls, either wall functions were employed or the no-slip condition and $k = 0$ in the two-layer calculations, while at the upper boundary of the channel wall functions were always used. In a separate calculation, fully developed channel flow was calculated first and the results were then used as inflow conditions. At the exit, zero gradient conditions were applied.

7. Results and discussions

Fig. 3 shows a comparison of streamlines in the plane of symmetry (left) and near the channel floor (right), while Table 1 compares various parameters characterizing the size and location of separation regions as defined in Fig. 2. The experimental results are time-averaged over a long period, and in Table 1 results of an LES calculation [6] are also included. From Fig. 3 it appears that the stagnation point is well simulated by the various models ($Y_s/H = 0.76$). The primary upstream separation location X_f (labelled A in the experimental flow pattern) which is caused by the strong pressure gradient imposed by the obstacle on the oncoming boundary layer is predicted differently by the wall function (WF) and two-layer (TL) models. The WF models predict the separation point (X_f) too close to the obstacle while the TL models give good agreement with experiments, with the exception of the TLV model which predicts somewhat early separation similar to the LES of Ref. [6]. The location of the horse-shoe vortex centre in front of the cube is well captured by the various TL models (at $X \approx -0.35$) while the WF-based models predict the centre further upstream. Also, the TL models are able to reproduce the secondary vortex developing right, in the corner in front of the obstacle (band labelled C) but the resolution of the streamline picture is not good enough to display this. The observations for the adverse pressure-gradient flow region in front of the obstacle allow the conclusion that here the TL models are clearly superior to the ones using wall functions.

Looking now at the separation region on the roof, it can be observed that the k–ε model with wall functions produces a much too small separation zone with unrealistic reattachment on the roof. When the KL modification is switched on, the separation region becomes much longer and in fact there is now no reattachment, but the separation bubble is too thin compared with the experimentally observed one. This improvement is brought about by the significant reduction of the turbulence kinetic energy produced in front of the obstacle, as can be seen from the k-contours given in Fig. 4. As a consequence, in the KL version there is less turbulence swept around the front corner so that the eddy viscosity over the roof is smaller, leading to a longer separation region. A similar effect is brought about by switching from WF to TL models (without KL modification) which also produce a separation bubble without reattachment which is, however, also too thin.

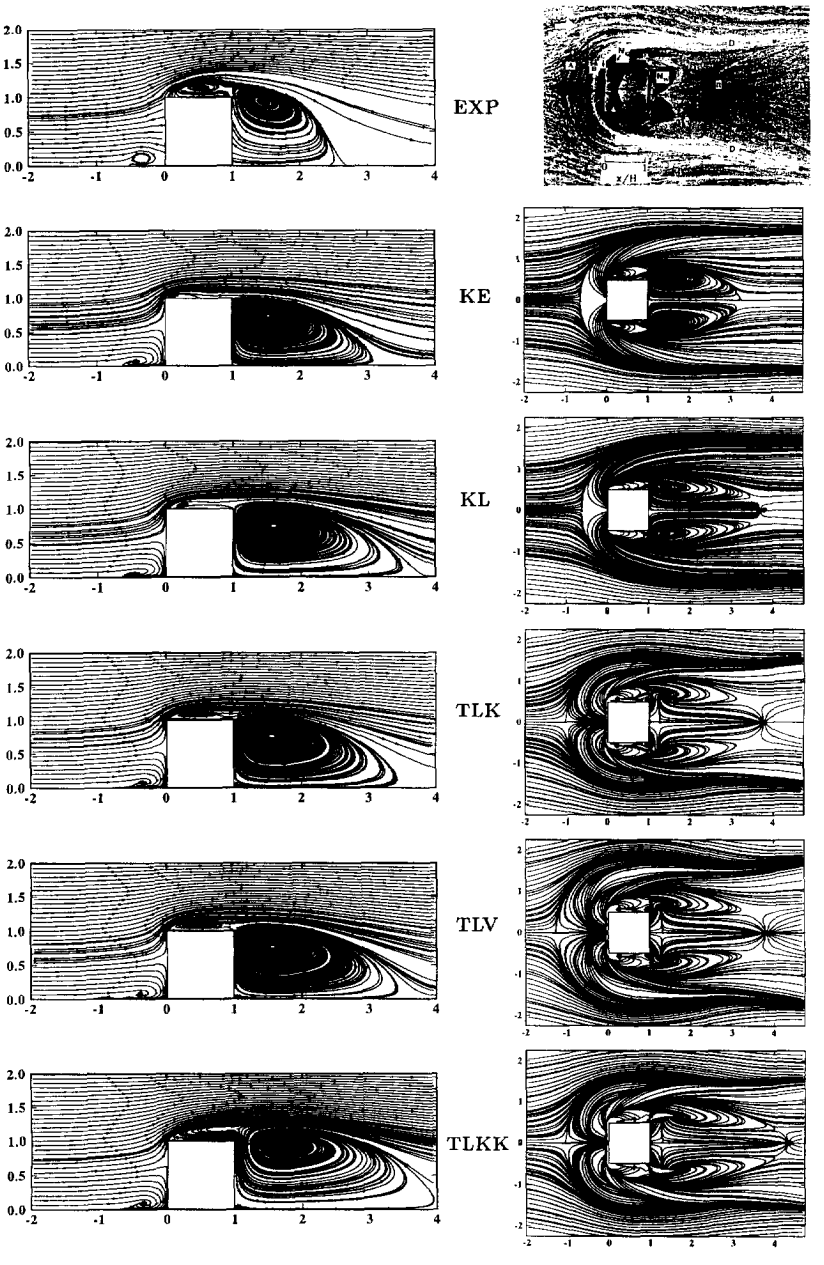

Fig. 3. Streamlines in the symmetry plane (left) and in the channel floor (right).

Table 1
Predicted flow structure parameters over the obstacle

Model	Key	Y_r	X_f	X_r	X_b
Experiment Ref. [2]	Exp	0.17	1.040	—	1.612
k–ε + (WF)	K-E	—	0.651	0.432	2.182
k-ε K–L + (WF)	KL	0.062	0.640	—	2.730
Two-layer k–ε	TLK	0.098	0.950	—	2.680
Two-layer k–ε	TLV	0.102	1.215	—	2.685
Two-layer k–ε	TLKK	0.160	0.950	—	3.405
LES [6]	LES-S	0.162	1.287	—	1.696
LES [6]	LES-D	0.162	0.998	—	1.432

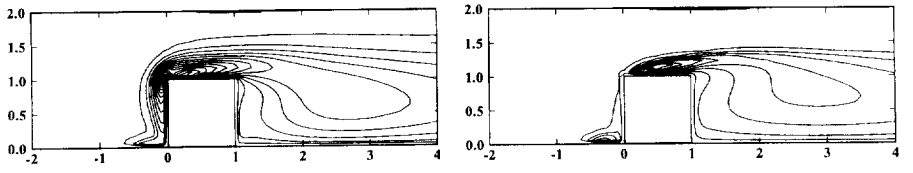

Fig. 4. k-isolines in the symmetry plane, left: KE; right: KL.

This improvement is due to the better resolution of the relatively thin bubble and the more realistic treatment of the near-wall region and is fully in line with previous observations made in 2D calculations (e.g. Ref. [4]). Combining the two-layer approach with the KL modification (TLKK) brings the predicted flow behaviour over the roof closest to the experimental one, i.e., the bubble thickness is now fairly realistic and clearly the separation region on the roof merges with that behind the obstacle. However, the centre of the bubble is predicted somewhat too far downstream. The Kato–Launder modification becomes, of course, more important the higher the approach-flow turbulence is. A recent calculation performed for a similar flow but with a higher turbulence intensity at roof height ($T_u = 0.16$) has shown that using the two-layer approach alone (TLK model) did not prevent unrealistic reattachment of the flow on the roof [14].

From Fig. 3 and Table 1 it is clear that the extension of the separation region behind the cube (X_b) is overpredicted by all models. The standard k–ε model with wall functions gives the smallest value and is closest to the experiments; both the introduction of the KL modification and the two-layer approach increase further the length of the separation region, and a combination of the two approaches (TLKK) gives the most excessive length ($X_b/H = 3.4$ compared with 1.62 in the experiments). As was discussed above, the KL modification reduces the k-production in front of the cube so that less turbulence is swept over the roof and also into the downstream region, leading to lower eddy viscosity there. This explains the longer separation zone vis-à-vis the standard k–ε model calculations. Moving from WF calculations to TL

calculations, the resulting larger and also thicker separation zone on the roof of course also increases the separation zone behind the cube, and the lengthening of the separation region when introducing the TL approach is also consistent with a variety of calculations of 2D separated flows. With these, however, the change is in the right direction, whereas here already the basic model produces too long a separation region. As sketched in Fig. 2, the flow field behind the cube is very complex with complex strain fields and curvature effects; the still fairly simple eddy-viscosity k–ε model may not be able to cope with these phenomena and a Reynolds-stress-equation model may do a better job. However. a more serious deficiency of the calculation methods used may be the fact that they are steady and ignore any vortex-shedding effects. In the experiments, vortex shedding from the side walls was observed, and such shedding can contribute greatly to the momentum exchange in the wake and can thereby reduce significantly the length of the separation region behind obstacles. This became very clear in previous calculations of the flow past a square cylinder [15]. Also the fact that the LES calculations [6], which resolve large-scale unsteady motions, produce the correct separation length supports the notion that the omission of unsteady effects may be the main cause for the overprediction of the separation length.

Fig. 3 compares also the calculated streamlines near the channel floor with the experimental oil-flow picture. In comparison with the WF models, the two-layer approaches reproduce much more detail of the flow structure near the wall due to the finer resolution in this region. The figure shows that the horse-shoe vortex is generally predicted quite well by the different approaches. The outer limit of the wake region formed by the lateral arms of the horse-shoe vortex (line D in oil-flow picture) varies however between the different calculation approaches. In the experiment, the width of this wake decreases up to approximately the reattachment point X_b; then it increases again. This feature governed by the rate of rolling is well described by the two-layer models while in contrast the WF model calculations do not produce the converging-diverging behaviour. The two-layer approaches also seem to predict correctly the corner vortices ($N12$) generated downstream of the vertical leading edges of the cube at the channel/obstacle junction. The location of the simulated arch vortices behind the obstacle ($N14$) shows clearly the differences between WF and TL results. In the k–ε WF calculations, basically the whole separation region is occupied by these vortices which contradicts the experimental observation; in the TL calculations these vortices are limited to a smaller area as in the experiments and as predicted similarly by the LES method. Since the large-eddy simulation produces nearly the correct separation length, it yields overall a flow pattern at the channel floor which is in very good agreement with the observed one.

Fig. 5 displays calculated and measured U-velocity profiles at different streamwise locations on the symmetry plane. All streamwise velocity profiles agree well with the measurements at $x/H = -1.0$ upstream of the cube. As was to be expected from the streamlines in Fig. 3, significant differences between the k–ε model results and the other results can already be observed at a location at the middle of the roof ($x/H = 0.5$). Here, and also at the position of the back face of the cube ($x/H = 1.0$), the TL results are in better agreement with the experiments; the best results were obtained with the TLKK model. The KL model performance is similar to that of TLK and

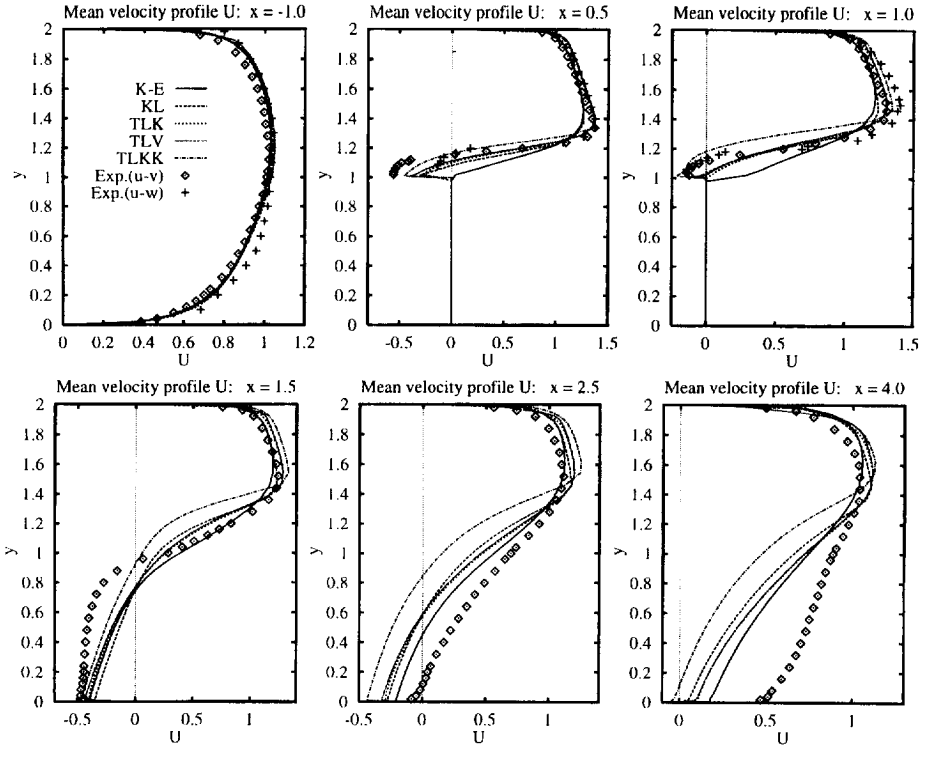

Fig. 5. Comparison of mean velocity profiles U in the symmetry plane.

TLV models, as was to be expected from the streamline pictures. At $x/H = 1.5$, the profiles predicted by the various models are rather similar and agree fairly well with the experiments in the region above the roof height. Below this, the reverse-flow velocity is underpredicted by all models. The further development of the U-profile is of course influenced mainly by the fact that the models predict too large a separation region so that the recovery is underpredicted by various degrees, of course worst by the TLKK model. Here, the LES calculations show much better agreement with the experiments.

Fig. 6 displays three vertical profiles of the shear stress $u'v'$ and turbulent kinetic energy k in the symmetry plane. At $x/H = 0.5$, all models using the TL approach predict fairly well the peak values of $u'v'$ and k except for TLKK which is low, while near the backward edge of the cube, these values are underpredicted by all models. This trend continues further downstream; in the region close to the flow reattachment point ($x/H = 2$ and 2.5) all models behave in a very similar way: the $u'v'$- and k-levels are underpredicted when compared with the experiments. This could partly be due to deficiencies of the eddy-viscosity concept but may again be largely caused by unsteady effects as the LES calculations produce higher levels in significantly better agreement with the measurements.

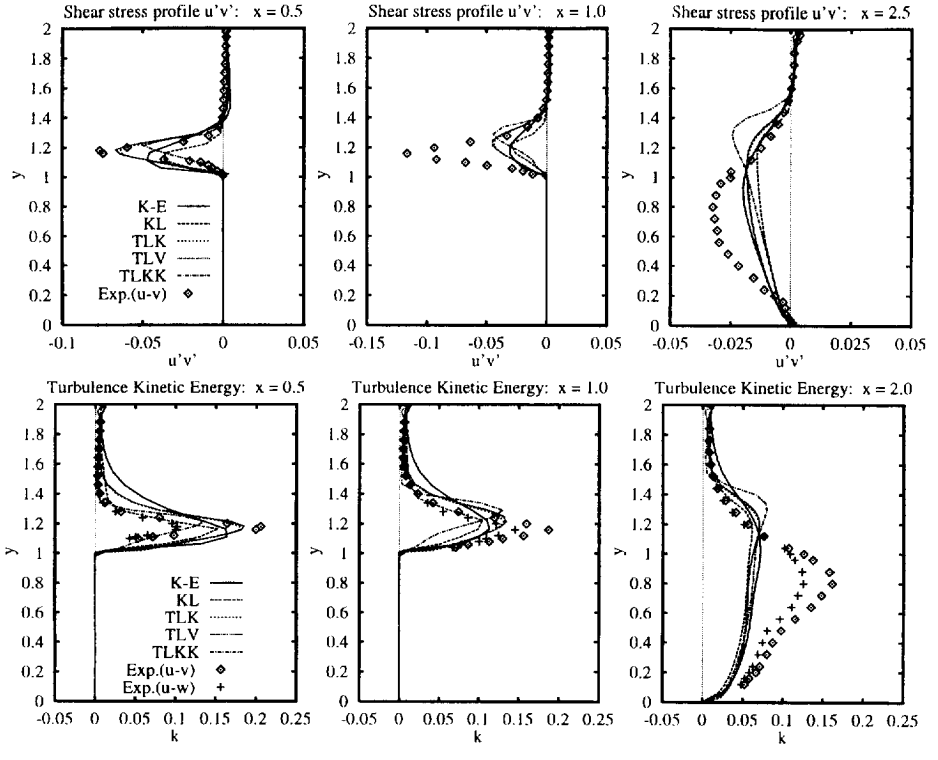

Fig. 6. Comparison of $u'v'$- and k-profiles in the symmetry plane.

8. Conclusions

Turbulent flow past a surface-mounted cubical obstacle placed in developed-channel flow has been investigated with various versions of the k–ε model, including different two-layer approaches, wall function treatment and the Kato–Launder modification. Despite the simple geometry of the obstacle, the flow developing in its vicinity is very complex with multiple, unsteady separation regions, vortices of various kinds, strong curvature and adverse as well as favourable pressure gradients. The models using wall functions cannot reproduce the details of the complex flow structure near the ground, e.g., the converging-diverging behaviour of the horse-shoe vortex, and also produce late separation of the boundary layer ahead of the obstacle. The standard version of the k–ε model further produces a much too small separation region with unrealistic reattachment on the roof. The simulation of this region is improved significantly by including the KL modification which eliminates the excessive kinetic energy production in the stagnation region. Using the two-layer approach, the details of the complex flow structure near the ground wall including the converging-diverging behaviour of the horse-shoe vortex can be resolved much better, the separation location in front of the cube is predicted correctly and also the prediction

of the separation region on the roof is improved – when combined with the KL modification the size of the roof separation bubble is predicted fairly well. The price for these improved predictions is, however, quite high since the computing time necessary was a factor of 25 larger than when wall functions were used. The calculations have shown also that, except for the adverse pressure gradient region in front of the obstacle, there is little difference in the results obtained with the TLK and TLV versions of the two-layer model. This indicates that, for the type of flow considered, the calculations are not sensitive to the details of the near-wall one-equation model. This conclusion is supported further by an additional calculation which has been performed using the TL model of Chen and Patel [16] which produced virtually the same results as the TLK model.

All models were found to overpredict the length of the separation region behind the cube, and introducing the Kato–Launder modification and the two-layer approach, which improve the predictions in the front part, both have an adverse effect on the separation length. It would be intriguing to see how Reynolds-stress-equation models perform, but it is likely that the unsteady effects such as the observed vortex shedding from the side walls significantly contribute to the momentum exchange and that the neglect of such effects in the steady calculations has led to the overprediction of the separation length. This notion is supported by the LES results [6] which produced good agreement with the experiments in every respect including the separation length. However, a very high price has to be paid for this as the LES calculations took 160 CPU hours on a SNI S600/20 vector computer while the two-layer model calculations took 6 h and the calculations using wall functions only 15 min.

Acknowledgements

The work reported here was sponsored by the Human Capital and Mobility Programme of the European Union. The calculations were carried out on the SNI S600/20 vector computer of the University of Karlsruhe (Computer Centre).

References

[1] M. Kato, B.E. Launder, The Modeling of turbulent flow around stationary and vibrating square cylinders, Proc. 9th Symp. on Turbulence and Shear Flows, Kyoto, 1993.

[2] R. Martinuzzi, C. Tropea, The flow around surface-mounted prismatic obstacle placed in a fully developed channel flow, J. Fluids Eng. 115 (1993) 85–92.

[3] W. Rodi, N.N. Mansour, Low Reynolds number k–ε modelling with the aid of direct numerical simulation data, J. Fluid Mech. 250 (1993) 509–529.

[4] J.Ch. Bonnin, T. Buchal, W. Rodi, ERCOFTAC workshop on data bases and testing of calculation methods for turbulent flows, University of Karlsruhe, 3–7 April 1995, ERCOFTAC Bull. 28 (1996) 48–54.

[5] W. Rodi, Experience with two-layer models conbining the k–ε model with a one-equation model near the wall, AIAA paper, AIAA-91-0216, 1991.

[6] M. Breuer, D. Lakehal, W. Rodi, Flow around a surface mounted cubical obstacle: comparisons of LES and RANS-Results, in: Computation of Three-Dimensional Complex Flows, M. Deville, S. Gavrilakis, I.L. Rhyming (Eds.), in: Notes of Numerical Fluid Mechanics, vol. 53, Vieweg Verlag, Braunschweig, 1996, pp. 22–30.

[7] B.E. Launder, D.B. Spalding, The numerical computation of turbulent flows, Comput. Meth. Appl. Mech. Eng. 3 (1974) 269–289.
[8] L.H. Norris, W.C. Reynolds, Turbulent channel flow with a moving wavy boundary, Report No. FM-10, Stanford University, Department Mechanical Engineering, 1975.
[9] W. Rodi, N.N. Mansour, V. Michelassi, One-equation near-wall turbulence modeling with the aid of direct simulation data, J. Fluids Eng. 115 (1993) 196–205.
[10] S. Majumdar, W. Rodi, J. Zhu, Three-dimensional finite-volume method for incompressible flows with complex boundaries, J. Fluids Eng. 114 (1992) 496–503.
[11] C.M. Rhie, W.L. Chow, A numerical study of the turbulent flow past an isolated airfoil with trailing edge separation, AIAA J. 21 (1983) 1225–1532.
[12] J. Zhu, A low-diffusive and oscillating-free convective scheme, Commun. Appl. Numer. Meth. 7 (1991) 225–232.
[13] H.L. Stone, Iterative solution of implicit approximations of multidimensional partial differential equations, SIAM J. Numer. Anal. 5 (1968) 530–558.
[14] D. Delaunay, D. Lakehal, C. Barré, C. Sacré, Numerical and wind-tunnel simulation of gas dispersion around a rectangular building, in: Proc. 2nd Int. Symp. on Computational Wind Engineering, Fort Collins, Colorado, 1996.
[15] R. Franke, W. Rodi, Calculation of vortex shedding past a square cylinder with various turbulence models, in: Durst et al. (Eds.), Turbulent and Shear Flows, vol. 8, Springer, Berlin, 1993, pp. 189–204.
[16] H.C. Chen, V.C. Patel, Near-wall turbulence models for complex flows including separation, AIAA J. 26 (1988) 641–648.